https://doi.org/10.1016/j.atmosres.2015.11.015

Chemical characterization and source apportionment of size-resolved particles in Hong Kong sub-urban area

Yuan Gao[1], Shun-Cheng Lee[1]*, Yu Huang[2], Judith C. Chow[2, 3], John G. Watson[2, 3]

[1] Department of Civil and Environmental Engineering, Research Institute for Sustainable Urban Development, The Hong Kong Polytechnic University, HungHom, Kowloon, Hong Kong SRA;
[2] Key Lab of Aerosol Chemistry & Physics，Institute of Earth Environment, Chinese Academy of Sciences，Xi'an, 710075, China
[3] Division of Atmospheric Sciences, Desert Research Institute, 2215 Raggio, Parkway, Reno, NV89512, USA

Submitted on 21st, July 2015

Atmospheric Research

Revised on 20th, October, 2015

* Corresponding author, Tel: 852 -2766 -6011; Fax: 852-2334 6389.
E-mail address: ceslee@polyu.edu.hk

Abstract

Size-resolved particulate matter (PM) samples were collected with a 10-stage Micro-Orifice Uniform Deposit Impactor (MOUDI) at a sub-urban site (Tung Chung) in Hong Kong for four non-consecutive months representing four seasons from 2011 to 2012. Major chemical components were water-soluble anions (i.e., Cl^-, NO_3^-, and SO_4^{2-}), cations (i.e., NH_4^+, Na^+, K^+, and Ca^{2+}), organic and elemental carbon and elements. Both chemical mass closure and positive matrix factorization (PMF) were employed to understand the chemical composition, resolve particle size modes, and evaluate the PM sources. Tri-modal size distributions were found for PM mass and major chemical components (e.g., SO_4^{2-}, NH_4^+, and OC). Mass median aerodynamic diameters (MMADs) with similar standard deviations ($1.32 < \sigma < 1.42$) were 0.4, 0.7 and 3.8 μm, consistent with condensation, droplet and coarse modes. A bi-modal distribution peaking at condensation and droplet modes was found for EC, with a single mode peaking at 3.8 μm for Cl^-. Besides secondary SO_4^{2-}, carbonaceous aerosol dominated the condensation mode with 27% by engine exhaust and 18-19% each by residual oil combustion (shipping) and coal/biomass burning. Secondary SO_4^{2-} is also the most dominant component in the droplet mode, accounting for 23% of PM mass, followed by an industrial source (19%). Engine exhaust, secondary NO_3^-, and sea salt each accounted for 13-15% of PM mass. Sea salt and soil are the dominated sources in the coarse mode, accounting for ~80% of coarse mass.

Keywords: Aerosol size distribution, inorganic ions, carbonaceous aerosol, MOUDI, PMF

65 # 1. INTRODUCTION

66 Airborne particulate matter (PMs) scatters and absorbs sunlight, causing direct
67 and indirect effects on Earth's radiation balance, visibility impairment, climate change,
68 and human health (Penttinen et al., 2001; Seinfeld and Pandis, 2006; Watson, 2002).
69 These effects are related to particle sizes and chemical compositions (Huang and Yu,
70 2008; Malm and Pitchford, 1997; Milford and Davidson, 1987; Sloane et al., 1991).
71 Based on size-resolved measurements from a Micro-Orifice Uniform Deposition
72 Impactor (MOUDI), Sloane (1983) and others quantified scattering efficiencies based
73 on Mie theory (Sloane et al., 1991; Sloane and Wolff, 1985). Major chemical
74 components (e.g., sulfate [SO_4^{2-}], nitrate [NO_3^-], and organics) have been used to
75 understand the particle growth mechanisms as well as the physical and chemical
76 characteristics (Howell and Huebert, 1998; Huang et al., 2006a; John et al., 1990;
77 Kim et al., 2003; Plaza et al., 2011; Tang, 1996; Tsai et al., 2012; Wang et al., 2013).

78 Past studies in Hong Kong have showed high concentration for SO_4^{2-}, organic
79 matter (OM), and elemental carbon (EC) in the submicron-mode, greatly influence
80 local visual range and human health (Gao et al., 2015; Yao et al., 2002; Yao et al.,
81 2003b; Zhuang et al., 1999b), similar to observations from other countries (John et al.,
82 1990; Kim et al., 2003; Plaza et al., 2011). Chow et al. (2008) observed a SO_4^{2-} size
83 distribution that was multi-modal and wider at an urban site than the uni-modal
84 distribution found at a rural site in central California. Bian et al (2014) found
85 significant size distribution changes over the past 20 year periods when compared the
86 three inorganic compounds (i.e., SO_4^{2-}, NO_3^-, and NH_4^+) at the same site. $PM_{2.5}$ or

87 PM_{10} source apportionment studies have been conducted in Hong Kong via different
88 receptor models (Fung and Wong, 1995; Guo et al., 2009; Lee et al., 1999), e.g.
89 Multivariate regression analysis, Principal Component Analysis with Absolute
90 Principal Component Scores technique (PCA-APCS), Chemical Mass Balance (CMB),
91 and Positive Matrix Factorization (PMF), finding contributions from engine exhaust,
92 secondary aerosols, residual oil combustion, fresh and aged sea salt, soil, coal
93 combustion and biomass burning. Only few source apportionment studies investigated
94 have examined contribution to different size ranges (Contini et al., 2014; Han et al.,
95 2006; Kim et al., 2003), but not in Hong Kong.

96 The Tung Chung (TC) site is a newly developed sub-urban area in Hong Kong,
97 located in the centerline of the Pearl River Delta (PRD) region. It is a gate way to
98 Macau and mainland China, with ~ 78,400 in habitants (*2011Census*) and increasing
99 industrial and commercial activities, such as coal-fired power plants, airports, seaports,
100 and local traffic (Wang et al., 2005; Zhou et al., 2014). Therefore, it is essential to
101 understand the air pollution in this area.

102 The objectives of this study are to: 1) investigate the particle size distribution of
103 water-soluble ions and carbon; and 2) determine resolved size mode and source
104 apportionment by the Positive Matrix Factorization (PMF) receptor model applied to
105 MOUDI (Model 110, MSP Corp. Minnesota, U.S.A.) data.
106
107
108
109

2. METHODS

2.1 Sampling site and sampling periods

The TC site (22.17 ^{o}N, 113.56 ^{o}E) is on the northern coast of Lantau Island and southwest of Hong Kong (Fig. 1). It is a new town area, ~3 km from the Hong Kong International Airport. MOUDI samplers were placed on a three storey building which was established by Hong Kong Environmental Protection Department (HKEPD). Sampling was conducted for 27 days cover four periods: August/September (2011), November/December (2011), February/March (2012), and May (2012), representing summer, fall, winter, and spring seasons, respectively. Sample duration was 24 hours, from 10:00 a.m. to 10:00 a.m. the next day local standard time (LST). Table 1 details the sampling dates and daily meteorological conditions.

2.2 Size-resolved particle measurements

The ten-stage MOUDI includes the following aerodynamic particle diameter ranges with 30 L/min flow rate: 0.056-0.1, 0.1-0.18, 0.18-0.32, 0.32-0.56, 0.56-1.0, 1.0-1.8, 1.8-3.2, 3.2-5.6, 5.6-10, and 10-18 μm. One MOUDI contained 47 mm Teflon-membranes Filters (Pall Sciences, New York, U.S.A.) and another contained 47 mm quartz-fiber filters (QMA, Whatman, Maidtone, England) as substrates. Backup filters were 37 mm. The spacer (0.05 inch in thickness) provided by MSP Corp. (MN, U.S.A.) was placed between adjacent stages to compensate for the lower jet-to-plate distance caused by the filter thickness (Huang et al., 2006b; Bian et al., 2014). Fujitani et al., (2006) reported that quartz-fiber filter artifacts are minimal

compared with aluminum foils or Teflon-membrane filter for PM concentrations of ~42 μg/m^3.

Ions and carbon were analyzed on quartz-fiber filters with mass and elements analyzed on Teflon-membrane filters. During the sampling periods, the effect of particle bounce should be negligible since the relative humidity (RH) was high, ~60% to 80% (Chow et al., 2005; Huang et al., 2004; Milford and Davidson, 1987).

Before sampling, quartz-fiber filters were prefired at 900 °C for three hours to minimize organic artifacts (Chow et al., 2010a; Ho et al., 2006; Watson et al., 2009). Both the Teflon-membrane and quartz-fiber filters were weighed before and after sampling, using a microbalance (Model MC5, Satorius, Goettingen, Germany) with a sensitivity of ±1 μg in the 0-250 mg range. Before weighing, filters were equilibrated in a desiccator for 24 hours at temperature (25 ± 5 °C) and RH (35 ± 10%) controlled environment. After weighing, filters were stored air-tight in a refrigerator (< 4 °C) to minimize evaporation of volatile components. Sample flow rates within ±10% of the specification were verified at the beginning and end of each sampling period.

2.3 Chemical Analysis

After gravimetric analyses, Teflon-membrane filters were analyzed for 51 elements (from Na to U) at the Institute of Earth and Environment, Chinese Academy of Science, China, by energy-dispersive X-Ray Fluorescence (XRF) analyses (Epsilon 5 ED-XRF, PANalytical B. V., the Netherlands, Watson et al., 1999). The quartz-fiber filters were analyzed for carbon fractions and water-soluble ions at the Air Laboratory

of the Hong Kong Polytechnic University (HKPU). A punch from each quartz-fiber filter (0.526 cm^2) was used for organic and elemental carbon (OC and EC) analysis using a DRI Model 2001 Thermal/Optical Carbon Analyzer (Atmoslytic Inc, Calabasas, CA, USA), following the IMPROVE_A-thermal/optical reflectance (TOR) protocol (Chow et al., 2011; Chow et al., 2007). For ion analysis, half of each quartz-fiber filter was extracted in 10 ml of ultra-pure deionized distilled water (specific resistance ≥18.1MΩ, Millipore). Extraction solutions were filtered and stored in plastic vials in a refrigerator (< 4 °C) until analysis. Water soluble ions including chloride (Cl^-), nitrate (NO_3^-), sulfate (SO_4^{2-}), sodium (Na^+), potassium (K^+), calcium (Ca^{2+}), and ammonium (NH_4^+) were analyzed by ion chromatography (ICS3000, DIONEX, Sunnylvale, C.A., U.S.A.) (Chow and Watson, 1999).

Reconstructed mass equation by chemical mass closure method, including soil, inorganic ions (i.e., SO_4^{2-}, NO_3^-, and NH_4^+), a biomass burning marker (K^+), EC, OM, trace element oxides (TEO) and sea salt (Chow et al., 2015; Chow et al., 2010b; Kong et al., 2014; Kumar et al., 2008; Malm et al., 1994; Sisler et al., 1996; Zhang et al., 2013) as follows:

Soil = 2.2×Al+2.49×Si+1.63×Ca+2.42×Fe+1.94×Ti (Malm et al., 1994) (1)

Particulate Organic matters (POM) =1.8 × OC (Hand et al., 2011) (2)

Trace element oxide (TEO) =1.3 × [0.5 × $(Sr + Ba + Mn + Co + Rb + Ni + V)$ + 1.0 × $(Cu + Zn + Mo + Cd + Sn + Sb + TI + Pb + As + Se + Ge + Cs + \mathrm{Ga})$] (Zhang et al., 2013) (3)

177 Sea salt = $1.47 \times Na^+ + Cl^-$ (Kong et al., 2014) (4)

178

179 ***2.4 PMF model***

180 Positive matrix factorization (PMF) model version 3.0 was used to resolve different
181 size modes and identify potential sources. Many previous studies have successfully
182 applied this factor analysis method to resolve the overlapping peaks (Guo et al., 2010;
183 Huang et al., 2006c; Kim et al., 2003). MOUDI size distribution data was viewed to
184 be data matrix X of sample *i* by *j* dimensions:

185

186 $$X_{ij} = \sum_{k=1}^{p} g_{ik} f_{kj} + e_{ij} \quad (5)$$

187

188 where *i* is the number of the samples, and *j* is the MOUDI stages (or chemical
189 species). Total factors *p* would be the resolved modes, g_{ik} is mass contribution of each
190 factor *k* to the individual sample *i*, f_{kj} is the species profile *j* of each source factor *k*,
191 and e_{ij} is the residual for each sample *i* or species *j*.

192 The measured chemical species concentration and their equation-based
193 uncertainties files should input into the model for further analysis. Detailed
194 calculation method for chemical species uncertainties are explained in the PMF user's
195 manual and by Tan et al., (2014; 2016). When a species concentration is below
196 detection limits for more than 50% of the samples, that species is excluded (Yau et al.,
197 2013). Chemical species were categorized as "strong", "weak", and "bad" (Paatero
198 and Tapper, 1994; Watson et al., 2015). S/N ratios > 2 were categorized as "strong"

and ratios between 0.2 and 2 were categorized as "weak". S/N ratios < 0.2 were assigned to the "bad" category and were excluded in the PMF analysis.

The number of factors should represent the actual sources situation, although there are sources mixing within factors. The Q value used to determine how well the factors and contributions reproduce the input, which should approximately equal the number of freedom degree or approximately equal to the data points in the data group (Polissar et al., 1998; Yau et al., 2013; Tan et al., 2014).

3. RESULTS AND DISCUSSION

3.1 Particle mass and major chemical compositions

Temporal variations of PM mass concentrations in Fig. 2, show large day-to-day variations with higher concentration found during fall and winter. The droplet mode (0.56 -1.8 μm) shows the largest contribution, accounting for 27-59% of PM_{10} mass, followed by the condensation mode (0.1 - 0.56 μm) and coarse modes (1.8 - 10 μm) in the range of 10-42% and 10-34% of PM_{10}, respectively. Table 2 summarizes daily average $PM_{1.8}$ and PM_{10} concentrations for the four seasons. Seasonal average $PM_{1.8}$ and PM_{10} varied from 26 and 39 $\mu g/m^3$ in spring to 37 and 53 $\mu g/m^3$ in fall, respectively. The highest average concentration (80 ± 13 $\mu g/m^3$) was found during summer hazy days, with a $PM_{1.8}/PM_{10}$ ratio of 0.78 ± 0.04. As shown in Table 2, both $PM_{1.8}$ and PM_{10} concentrations increased by 3-4 fold during pollution episodes, but the ratio of $PM_{1.8}$ to PM_{10} decreased from 0.83 ± 0.02 (clean days) to 0.78 ± 0.04 (episode days), indicating increasing particle sizes for the polluted days.

Approximately 39% of samples exceeded the 24-hour PM_{10} standard/guideline of 50 $\mu g/m^3$ in Europe and WHO. $PM_{1.8}$ and PM_{10} concentrations were ~20 - 60% lower than those at urban sites in Hong Kong (Chow et al., 2010b; Ho et al., 2006; Louie et al., 2005). Comparable $PM_{2.5}$ concentrations were found at the Tai'O (41 $\mu g/m^3$) and Tung Chung (37 $\mu g/m^3$) sites (Cheung et al., 2005), with fine particle to PM_{10} ratios averaging 0.72 ± 0.09, and ranging from 0.46 to 0.88.

The reconstructed PM_{10} mass for each season in Fig. 3 shows a high correlation (R = 0.8~0.97) with gravimetric PM_{10} mass. SO_4^{2-} is the most abundant species, accounting for 26 - 37% of PM_{10} mass. POM is the second largest component, constituting 8 - 10% of PM_{10} during spring and winter to 24 - 29% during fall and summer. NO_3^- accounts for 14-16% of PM_{10} in fall and winter, reduced to ~8% in spring and ~3% in summer. Some NO_3^- maybe volatized during warm seasons. Sea salt contributed its largest fraction in spring (~31%) and was lowest in winter (11%). Sea salt fractions of PM_{10} during summer and fall were ~ 14%. Soil contribution ranged from 5% in spring to 10 - 11% in summer and fall. There are no apparent seasonal variations for NH_4^+ (2 - 5%), EC (5%), TEO (1 - 2%), and K^+ (0 - 1%). Differences between reconstructed and measured PM_{10} (i.e., others) were higher in winter and spring (9-18%), which could be attributed to sampling and analysis uncertainties (Chow et al 2015).

3.2 Resolved particle size distribution modes

PMF has been used to resolve particle size distributions by Garrido Frenich et al., (2000), Huang et al., (2006a; 2006c), Kim et al., (2003) and Yu et al., (2010). The nucleation, condensation, droplet, and coarse modes, indicate PM origins and aging. Droplet mode particles form through aqueous reaction in clouds and fogs (Hering and Friedlander, 1982; Seinfeld and Pandis, 2006). A total of 161 samples (23 sets × 7 species (i.e., ions and carbon) and their equation-based uncertainties were used in PMF 3.0 software, with typical results shown in Fig. 4. Mass median aerodynamic diameter (MMAD) and standard deviation (σ) were 0.4 μm (σ=1.42), 0.7 μm (σ=1.32), and 3.8 μm (σ=1.38), respectively. The standard deviation (σ) illustrates the width of distribution; a lower σ value indicates narrower distribution. Similar MMADs and σ for condensation (0.34 ± 1.39 μm) and droplet (0.84 ± 1.39 μm) modes were observed in urban Shenzhen and Beijing, but the coarse mode MMADs were higher than those at TC, 5.4 ± 1.56 μm and 5.7 ± 1.39 μm, respectively (Guo et al., 2010; Lan et al., 2011).

Fig. 5 shows resolved size distributions for 7 species (i.e., SO_4^{2-}, NO_3^-, NH_4^+, Cl^-, K^+, OC, and EC). Tri-modal size distributions were found for SO_4^{2-}, with one dominated peak in the droplet mode (0.8 μm, σ=1.2), and small peaks for the condensation and coarse modes (Fig. 5a). The SO_4^{2-} size distribution is consistent with: 1) a condensation mode formed by gas-to-particle conversion (e.g., photochemical oxidation of sulfur dioxide (SO_2) (Lan et al., 2011; Seinfeld and Pandis, 2006); 2) a droplet mode formed by aqueous SO_2 oxidation (John et al., 1990;

Kerminen and Wexler, 1995; Zhuang et al., 1999b); and 3) a coarse mode formed by reactions with sea salt or soil (Zhuang et al., 1999a). The resolved SO_4^{2-} size distribution is similar to previous studies in Hong Kong and mainland China (Guo et al., 2010; Lan et al., 2011; Yao et al., 2003a; Zhuang et al., 1999b), attributing ~60% of SO_4^{2-} to in-cloud process, ~25% to gas-phase chemistry, and ~15% to reactions with soil and sea salt (R = 0.8, between Na^+ and SO_4^{2-}, in summer and fall).

In-cloud process and condensation onto pre-existing particles are also the potential pathways to form droplet and condensation NO_3^-. Thermodynamic equilibrium state is the dominant factor that affect NO_3^- size distribution (John et al., 1990; Seinfeld and Pandis, 2006), where:

$$HNO_3\ (g) + NH_3\ (g) \leftrightarrow NH_4NO_3\ (s, aq) \quad (6)$$

When the gaseous ammonia (NH_3) and nitric acid (HNO_3) is larger than the equilibrium constant, the ammonium nitrate (NH_4NO_3) will be presented (Zhuang et al., 1999b). Fig. 5b shows abundant coarse mode (~67% of NO_3^-), followed by droplet mode (~33%). Coarse mode NO_3^- results from the reaction of nitric acid (HNO_3) with alkaline sea salt and soil. Fine particle NO_3^- is semi-volatile and changes between gas and particle phases depending on ambient temperature and RH (Chow et al., 2008). This may explain why only a few condensation mode peaks were observed in this study.

SO_4^{2-} and NO_3^- contribution can be elucidated by the sulfur oxidation ratio (SOR)

and the nitrogen oxidation ratio (NOR):

$$SOR = \frac{[SO_4^{2-}]}{[SO_4^{2-}+SO_2]} \quad (7)$$

$$NOR = \frac{[NO_3^-]}{[NO_3^-+NO_2]}, \quad (8)$$

where SO_4^{2-}, sulfur dioxide (SO_2), NO_3^-, and nitrogen dioxide (NO_2) are molar concentrations in units of mol/m^3. Higher SOR and NOR values indicate that larger amounts of secondary SO_4^{2-} and NO_3^- particles were formed by photochemical oxidation of precursor gases (Kadowaki, 1986; Khoder, 2002). Fig. 6 shows the SORs and NORs for three size modes. The NORs are lower than SORs in spring and summer and higher in fall and winter, implying different SO_4^{2-} and NO_3^- formation and removal mechanisms. The seasonal pattern for SORs were opposite that for NORs. Higher temperatures in summer and spring (23 - 29 ^oC) favor the formation of SO_4^{2-} by photochemical oxidation, but these enhance the volatilization of NO_3^-. Correlations between SOR and temperature increase as particle size decreases. SOR is the highest for the droplet mode, ~60% higher than for the condensation and coarse modes. NOR is most abundant in the coarse mode as compared to condensation and droplet modes, suggesting the sea salt or soil formation of coarse particle NO_3^- (e.g., sodium nitrate and calcium nitrate). Reasonable correlation (R = 0.6) was found between RH and NOR, suggesting aqueous phase reactions under high RHs.

NH_4^+ and K^+ are mostly in the droplet mode (Figs. 5c and 5d). The molar ratio of NH_4^+ to SO_4^{2-} in fine mode was 1.0, indicating incomplete neutralization of

310 ammonium bisulfate and sulfuric acid (Liu et al., 2008). A similar K^+ size distribution
311 was found in Shenzhen and PRD region (Andreae, 1983; Huang et al., 2006a; Lan et
312 al., 2011; Novakov and Corrigan, 1996). Small peak of K^+ in coarse mode may due to
313 coagulation process of biomass burning emissions from small particles and sea salt
314 (Bian et al., 2014). A single coarse mode was found for Cl^- (Fig. 5e), indicative of the
315 presence of sea salt, similar to that found by Yao et al., (2003b).

316 EC in the condensation (0.28 μm) and droplet (0.8 μm) modes contributed 0.5 and
317 0.6 $\mu g/m^3$, respectively, consistent with fresh and slightly aged engine exhaust, similar
318 to those found in Shenzhen (Huang and Yu, 2008). Dominated droplet mode in EC
319 suggests aged EC which nucleated and condensed from fresh EC emissions. Some
320 correlation was found between EC and SO_4^{2-} ($R = 0.72$), may be related to fuel sulfur
321 contents, especially from heavy oils used in ocean-going vessels. Previous studies in
322 PRD region suggested internal mixed of EC and SO_4^{2-} and aqueous processes (Cheng
323 et al., 2006; Huang and Yu, 2008). Abundance of droplet mode was also apparent for
324 OC, followed by condensation mode. OC concentrations in the condensation, droplet,
325 and coarse modes are 1.9, 2.0 and 0.4 $\mu g/m^3$, respectively. The OC/EC ratios are > 2
326 in the droplet and condensation modes.

327

328 ***3.3 Pollution episodes***

329 There was one polluted episode occurred during summer, including one clean day,
330 on August 20th to 21st and two polluted days representing the beginning (August 24th
331 to 25th) and ending (August 29th to 30th) of the pollution episode (Fig. 7a). The ratio of

each particle size mode to PM_{10} changes significantly from clean day to the end of pollution episode day. On the polluted days, particles in the condensation mode decreased from ~31% to ~18%, with concurrent increases in the droplet mode from ~42% to 52%, and a partial increase (~19% to 24%) in the coarse mode. Chemical mass closure also showed major chemical components have significant differences. PM_{10} fraction of POM and EC for clean and episode ending days, reduced from 36% to 24%, suggesting a larger regional-scale contribution. The abundance of SO_4^{2-} in PM_{10} increased from 16% to 40%, showing secondary aerosol formation process dominated the episode period. Back trajectories were used to identify the origin of the sources during the clean and episode days. As shown in Fig. 7a, the clean day air mass originated from the ocean, bringing uncontaminated air to the TC. During the episode, polluted and stagnant air masses come from the PRD region.

The mass ratio of non seasalt-SO_4^{2-} (i.e., SO_4^{2-} - 0.253×Na^+) and NO_3^- can be used to indicate contribution acidity (Kong et al., 2014). The ratios of NSS-SO_4^{2-} and NO_3^- were increased significantly, from 2.3, 19, to 36 for clean, episode starting and episode ending days, respectively. Particle acidity during this episode period is more effected by SO_4^{2-} than NO_3^- (Kong et al., 2014). Fig. 7b shows a remarkable high SOR value in the droplet mode during the polluted days. Due to high temperature in summer, the NOR did not exhibit much change.

3.4 Source factors in condensation, droplet, and coarse modes

354 Source apportionment by PMF3.0 software was conducted for the three size modes
355 (i.e., condensation, droplet and coarse modes). Total of 69 (23 sets × 3 stages) filter
356 samples with their measured chemical species concentrations and associated
357 uncertainties were input into the model (Huang et al., 2006b). Table 3 and Fig. 8
358 summarize the nine source factors and their identifies markers (Choi et al., 2001; Han
359 et al., 2006; Senaratne and Shooter, 2004; Tan et al., 2014; Tan et al., 2016; Yau et al.,
360 2013). Similar to mass size distribution pattern in Fig.4, eight source factors were
361 found for the droplet mode, four source factors for the condensation mode, and three
362 for the coarse mode, as shown in Fig. 9. Sea salt and soil factors contributed > 80% of
363 the coarse mass. Anthropogenic sources contributed to the droplet mode, with 24%
364 from the secondary SO_4^{2-} factor, 19% from the industrial emissions factor and 13-15%
365 each from the engine exhaust, secondary NO_3^-, and sea salt factors. Other source
366 factors contributed 10% of the droplet mode particle mass concentrations. The
367 condensation mode had 37% contribution from the secondary SO_4^{2-} factor, 27% from
368 the engine exhaust factor, and 18-19% each from the residual oil combustion and
369 coal/biomass burning factors.
370
371 **4. CONCLUSIONS**
372
373 Size-segregated samples were collected by 10-stage Micro-Orifice Uniform Deposit
374 Impactor (MOUDI) for the four seasons: summer (August/September, 2011), fall
375 (November/December, 2011), winter (February/March, 2012), and summer (May,

2012). In addition to gravimetric mass, water-soluble ions, organic/elemental carbon, and elemental species were analyzed. The major chemical components were examined using chemical mass closure method. The size distribution of major chemical species and source apportionment on size-resolved modes were investigated using positive matrix factorization (PMF) model.

PM_{10} chemical composition varies by seasons. The highest PM_{10} concentrations are found in the fall with the lowest concentration in the spring. Secondary sulfate and organic matters (1.8×OC) were the two largest PM_{10} components, accounting for 26-37% and 8-30% of PM mass.

Tri-modal size distributions are found for SO_4^{2-}, NH_4^+ and OC, with mass median aerodynamic diameters (MMADs) of 0.4, 0.7, and 3.8 μm for the condensation, droplet and coarse modes, and a similar widths (i.e., standard deviation, σ, ranging 1.32 - 1.42). The droplet mode is most prominent for SO_4^{2-}, NH_4^+, K^+, OC, and EC. NO_3^- is more prominent in the coarse mode, whereas a single coarse mode is found for Cl^-.

The condensation mode mass is explained of 36% secondary SO_4^{2-} factor, 26% engine exhaust factor, along with 18-19% each for residual oil combustion and coal/biomass burning factors. Eight source factors contribution were in the droplet mode, with from 23% SO_4^{2-} factor, 19% from industrial emissions factor, and 14-16% each for engine exhaust, secondary NO_3^-, and sea salt factor. Approximately, 80% of coarse mode mass is attributed to sea salt and soil factors.

ACKNOWLEDGMENTS

The authors wish to acknowledge the financial support of the Environmental Conservation Fund of Hong Kong (7/2009) and the Research Grants Council of the Hong Kong Special Administrative Region (PolyU 152083/14E). We thank Professor Tao Wang and his group member of Hong Kong Polytechnic University, Dr. Kinfai Ho of the Chinese University of Hong Kong for their contribution on field study and Hong Kong Environmental Protection Department for providing gaseous data.

REFERENCES

Andreas, M.O., 1983. Soot carbon and excess fine potassium: Long-range transport of combustion-derived aerosols. Science 220, 1148-1151.

Bian, Q., Huang, X.H.H., Yu, J.Z., 2014. One-year observations of size distribution characteristics of major aerosol constituents at a coastal receptor site in Hong Kong – Part 1: Inorganic ions and oxalate. Atmos. Chem. Phys. 14, 9013-9027.

Cheng, Y.F., Eichler, H., Wiedensohler, A., Heintzenberg, J., Zhang, Y.H., Hu, M., Herrmann, H., Zeng, L.M., Liu, S., Gnauk, T., Brüggemann, E., He, L.Y., 2006. Mixing state of elemental carbon and non-light-absorbing aerosol components derived from in situ particle optical properties at Xinken in Pearl River Delta of China. Journal of Geophysical Research: Atmospheres 111, D20204.

Cheung, H.-C., Wang, T., Baumann, K., Guo, H., 2005. Influence of regional pollution outflow on the concentrations of fine particulate matter and visibility in the coastal area of southern China. Atmospheric Environment 39, 6463-6474.

Choi, J.C., Lee, M., Chun, Y., Kim, J., Oh, S., 2001. Chemical composition and source signature of spring aerosol in Seoul, Korea. Journal of Geophysical Research: Atmospheres 106, 18067-18074.

Chow, J., Lowenthal, D., Chen, L.W.A., Wang, X., Watson, J., 2015. Mass reconstruction methods for $PM_{2.5}$: a review. Air Quality, Atmosphere & Health 8, 243-263.

Chow, J., Watson, J., Robles, J., Wang, X., Chen, L.W.A., Trimble, D., Kohl, S., Tropp, R., Fung, K., 2011. Quality assurance and quality control for thermal/optical analysis of aerosol samples for organic and elemental carbon. Analytical and Bioanalytical Chemistry 401, 3141-3152.

Chow, J.C., Watson, J.G., 1999. Ion chromatography in elemental analysis of airborne particles. Elemental analysis of airborne particles Vol. 1, Chapter: 3, Publisher: Gordon and Breach Science, Amsterdam, The Netherlands, Editors: S. Landsberger, M. Creatchman, pp.97-137.

Chow, J.C., Watson, J.G., Chen, L.-W.A., Chang, M.O., Robinson, N.F., Trimble, D., Kohl, S., 2007. The IMPROVE_A temperature protocol for thermal/optical carbon analysis: maintaining consistency with a long-term database. Journal of the Air & Waste Management Association 57, 1014-1023.

Chow, J.C., Watson, J.G., Chen, L.W.A., Rice, J., Frank, N.H., 2010a. Quantification of $PM_{2.5}$ organic carbon sampling artifacts in US networks. Atmos. Chem. Phys. 10, 5223-5239.

Chow, J.C., Watson, J.G., Kohl, S., Chen, L.-W.A., Chai, W., 2010b. Measurements and validation for the 2008/2009 particulate matter study in Hong Kong. Reno, USA: Desert Research Institute. NV.

Chow, J.C., Watson, J.G., Lowenthal, D.H., Magliano, K.L., 2005. Loss of PM2.5 Nitrate from Filter Samples in Central California. Journal of the Air & Waste Management Association 55, 1158-1168.

Chow, J.C., Watson, J.G., Lowenthal, D.H., Magliano, K.L., 2008. Size-resolved

aerosol chemical concentrations at rural and urban sites in Central California, USA. Atmospheric Research 90, 243-252.
Contini, D., Cesari, D., Genga, A., Siciliano, M., Ielpo, P., Guascito, M.R., Conte, M., 2014. Source apportionment of size-segregated atmospheric particles based on the major water-soluble components in Lecce (Italy). Science of The Total Environment 472, 248-261.
Fujitani, Y., Hasegawa, S., Fushimi, A., Kondo, Y., Tanabe, K., Kobayashi, S., Kobayashi, T., 2006. Collection characteristics of low-pressure impactors with various impaction substrate materials. Atmospheric Environment 40, 3221-3229.
Fung, Y.S., Wong, L.W.Y., 1995. Apportionment of air pollution sources by receptor models in Hong Kong. Atmospheric Environment 29, 2041-2048.
Gao, Y., Lai, S., Lee, S.-C., Yau, P.S., Huang, Y., Cheng, Y., Wang, T., Xu, Z., Yuan, C., Zhang, Y., 2015. Optical properties of size-resolved particles at a Hong Kong urban site during winter. Atmospheric Research 155, 1-12.
Garrido Frenich, A., Martínez Galera, M., Martínez Vidal, J.L., Massart, D.L., Torres-Lapasió, J.R., De Braekeleer, K., Wang, J.-H., Hopke, P.K., 2000. Resolution of multicomponent peaks by orthogonal projection approach, positive matrix factorization and alternating least squares. Analytica Chimica Acta 411, 145-155.
Guo, H., Ding, A.J., So, K.L., Ayoko, G., Li, Y.S., Hung, W.T., 2009. Receptor modeling of source apportionment of Hong Kong aerosols and the implication of urban and regional contribution. Atmospheric Environment 43, 1159-1169.
Guo, S., Hu, M., Wang, Z.B., Slanina, J., Zhao, Y.L., 2010. Size-resolved aerosol water-soluble ionic compositions in the summer of Beijing: implication of regional secondary formation. Atmos. Chem. Phys. 10, 947-959.
Han, J., Moon, K., Lee, S., Kim, Y., Ryu, S., Cliff, S., Yi, S., 2006. Size-resolved source apportionment of ambient particles by positive matrix factorization at Gosan background site in East Asia. Atmospheric Chemistry and Physics 6, 211-223.
Hand, J., Copeland, D., Day, A., Indresand, D., Malm, W., McDade, C., Moore, C., Pitchford, M., Schichtel, B., Watson, J., 2011. Spatial and seasonal patterns and temporal variability of haze and its constituents in the United States: Report V: June 2011. Cooperative Institute for Research in the Atmosphere for the IMPROVE program, Ft. collins, Co.
Hering, S.V., Friedlander, S.K., 1982. Origins of aerosol sulfur size distributions in the Los Angeles basin. Atmospheric Environment (1967) 16, 2647-2656.
Ho, K.F., Lee, S.C., Cao, J.J., Chow, J.C., Watson, J.G., Chan, C.K., 2006. Seasonal variations and mass closure analysis of particulate matter in Hong Kong. Science of The Total Environment 355, 276-287.
Howell, S.G., Huebert, B.J., 1998. Determining marine aerosol scattering characteristics at ambient humidity from size - resolved chemical composition. Journal of Geophysical Research: Atmospheres (1984–2012) 103, 1391-1404.
Huang, X.-F., Yu, J.Z., He, L.-Y., Hu, M., 2006a. Size Distribution Characteristics of Elemental Carbon Emitted from Chinese Vehicles: Results of a Tunnel Study and

493 Atmospheric Implications. Environmental Science & Technology 40, 5355-5360.
494 Huang, X.F., Yu, J.Z., 2008. Size distributions of elemental carbon in the atmosphere
495 of a coastal urban area in South China: characteristics, evolution processes, and
496 implications for the mixing state. Atmospheric Chemistry and Physics 8,
497 5843-5853.
498 Huang, X.F., Yu, J.Z., He, L.Y., Hu, M., 2006b. Size distribution characteristics of
499 elemental carbon emitted from Chinese vehicles: Results of a tunnel study and
500 atmospheric implications. Environmental Science & Technology 40, 5355-5360.
501 Huang, X.F., Yu, J.Z., He, L.Y., Yuan, Z.B., 2006c. Water-soluble organic carbon and
502 oxalate in aerosols at a coastal urban site in China: Size distribution characteristics,
503 sources, and formation mechanisms. Journal of Geophysical
504 Research-Atmospheres 111.
505 Huang, Z., Harrison, R.M., Allen, A.G., James, J.D., Tilling, R.M., Yin, J., 2004. Field
506 intercomparison of filter pack and impactor sampling for aerosol nitrate,
507 ammonium, and sulphate at coastal and inland sites. Atmospheric Research 71,
508 215-232.
509 John, W., Wall, S.M., Ondo, J.L., Winklmayr, W., 1990. Modes in the size
510 distributions of atmospheric inorganic aerosol. Atmospheric Environment. Part A.
511 General Topics 24, 2349-2359.
512 Kadowaki, S., 1986. On the nature of atmospheric oxidation processes of sulfur
513 dioxide to sulfate and of nitrogen dioxide to nitrate on the basis of diurnal
514 variations of sulfate, nitrate, and other pollutants in an urban area. Environmental
515 Science & Technology 20, 1249-1253.
516 Kerminen, V.-M., Wexler, A.S., 1995. Enhanced formation and development of sulfate
517 particles due to marine boundary layer circulation. Journal of Geophysical
518 Research: Atmospheres 100, 23051-23062.
519 Khoder, M.I., 2002. Atmospheric conversion of sulfur dioxide to particulate sulfate
520 and nitrogen dioxide to particulate nitrate and gaseous nitric acid in an urban area.
521 Chemosphere 49, 675-684.
522 Kim, E., Hopke, P.K., Larson, T.V., Covert, D.S., 2003. Analysis of Ambient Particle
523 Size Distributions Using Unmix and Positive Matrix Factorization. Environmental
524 Science & Technology 38, 202-209.
525 Kong, S., Wen, B., Chen, K., Yin, Y., Li, L., Li, Q., Yuan, L., Li, X., Sun, X., 2014.
526 Ion chemistry for atmospheric size-segregated aerosol and depositions at an
527 offshore site of Yangtze River Delta region, China. Atmospheric Research
528 147–148, 205-226.
529 Kumar, A., Sarin, M.M., Sudheer, A.K., 2008. Mineral and anthropogenic aerosols in
530 Arabian Sea–atmospheric boundary layer: Sources and spatial variability.
531 Atmospheric Environment 42, 5169-5181.
532 Lan, Z.-J., Chen, D.-L., Li, X., Huang, X.-F., He, L.-Y., Deng, Y.-G., Feng, N., Hu, M.,
533 2011. Modal characteristics of carbonaceous aerosol size distribution in an urban
534 atmosphere of South China. Atmospheric Research 100, 51-60.
535 Lee, E., Chan, C.K., Paatero, P., 1999. Application of positive matrix factorization in
536 source apportionment of particulate pollutants in Hong Kong. Atmospheric

Environment 33, 3201-3212.
Liu, S., Hu, M., Slanina, S., He, L.Y., Niu, Y.W., Bruegemann, E., Gnauk, T., Herrmann, H., 2008. Size distribution and source analysis of ionic compositions of aerosols in polluted periods at Xinken in Pearl River Delta (PRD) of China. Atmospheric Environment 42, 6284-6295.
Louie, P.K.K., Chow, J.C., Chen, L.W.A., Watson, J.G., Leung, G., Sin, D.W.M., 2005. PM2.5 chemical composition in Hong Kong: urban and regional variations. Science of The Total Environment 338, 267-281.
Malm, W.C., Pitchford, M.L., 1997. Comparison of calculated sulfate scattering efficiencies as estimated from size-resolved particle measurements at three national locations. Atmospheric Environment 31, 1315-1325.
Malm, W.C., Sisler, J.F., Huffman, D., Eldred, R.A., Cahill, T.A., 1994. Spatial and seasonal trends in particle concentration and optical extinction in the United States. Journal of Geophysical Research 99, 1347-1370.
Milford, J.B., Davidson, C.I., 1987. The Sizes of Particulate Sulfate aed Nitrate 1B the Atmosphere—A-Review. JAPCA 37, 125-134.
Novakov, T., Corrigan, C.E., 1996. Cloud condensation nucleus activity of the organic component of biomass smoke particles. Geophysical Research Letters 23, 2141-2144.
Paatero, P., Tapper, U., 1994. Positive matrix factorization: A non-negative factor model with optimal utilization of error estimates of data values. Environmetrics 5, 111-126.
Penttinen, P., Timonen, K.L., Tiittanen, P., Mirme, A., Ruuskanen, J., Pekkanen, J., 2001. Ultrafine particles in urban air and respiratory health among adult asthmatics. European Respiratory Journal 17, 428-435.
Plaza, J., Pujadas, M., Gómez-Moreno, F.J., Sánchez, M., Artíñano, B., 2011. Mass size distributions of soluble sulfate, nitrate and ammonium in the Madrid urban aerosol. Atmospheric Environment 45, 4966-4976.
Polissar, A.V., Hopke, P.K., Paatero, P., Malm, W.C., Sisler, J.F., 1998. Atmospheric aerosol over Alaska: 2. Elemental composition and sources. Journal of Geophysical Research: Atmospheres 103, 19045-19057.
Seinfeld, J.H., Pandis, S.N., 2006. Atmospheric chemistry and physics: from air pollution to climate change. John Wiley & Sons.
Senaratne, I., Shooter, D., 2004. Elemental composition in source identification of brown haze in Auckland, New Zealand. Atmospheric Environment 38, 3049-3059.
Sisler, J.F., Malm, W., Gebhart, K., Pitchford, M.L., 1996. Spatial and Seasonal Patterns and Long Term Variability of the composition of the Haze in the United States. Report ISSN, 0737-5352, CIRA, Ft. Collins, Co.
Sloane, C.S., 1983. Optical properties of aerosols—Comparison of measurements with model calculations. Atmospheric Environment (1967) 17, 409-416.
Sloane, C.S., Watson, J., Chow, J., Pritchett, L., Willard Richards, L., 1991. Size-segregated fine particle measurements by chemical species and their impact on visibility impairment in Denver. Atmospheric Environment. Part A. General Topics 25, 1013-1024.

581 Sloane, C.S., Wolff, G.T., 1985. Prediction of ambient light scattering using a physical
582 model responsive to relative humidity: Validation with measurements from Detroit.
583 Atmospheric Environment (1967) 19, 669-680.
584 Tan, J.-H., Duan, J.-C., Ma, Y.-L., Yang, F.-M., Cheng, Y., He, K.-B., Yu, Y.-C., Wang,
585 J.-W., 2014. Source of atmospheric heavy metals in winter in Foshan, China.
586 Science of The Total Environment 493, 262-270.
587 Tan, J., Duan, J., Zhen, N., He, K., Hao, J., 2016. Chemical characteristics and source
588 of size-fractionated atmospheric particle in haze episode in Beijing. Atmospheric
589 Research 167, 24-33.
590 Tang, I.N., 1996. Chemical and size effects of hygroscopic aerosols on light scattering
591 coefficients. Journal of Geophysical Research: Atmospheres (1984–2012) 101,
592 19245-19250.
593 Tsai, J.-H., Lin, J.-H., Yao, Y.-C., Chiang, H.-L., 2012. Size distribution and water
594 soluble ions of ambient particulate matter on episode and non-episode days in
595 Southern Taiwan. Aerosol Air Qual. Res 12, 263-274.
596 Wang, T., Guo, H., Blake, D.R., Kwok, Y.H., Simpson, I.J., Li, Y.S., 2005.
597 Measurements of Trace Gases in the Inflow of South China Sea Background Air
598 and Outflow of Regional Pollution at Tai O, Southern China. Journal of
599 Atmospheric Chemistry 52, 295-317.
600 Wang, X., Wang, T., Pathak, R., Hallquist, M., Gao, X., Nie, W., Xue, L., Gao, J., Gao,
601 R., Zhang, Q., Wang, W., Wang, S., Chai, F., Chen, Y., 2013. Size distributions of
602 aerosol sulfates and nitrates in Beijing during the 2008 Olympic Games: Impacts
603 of pollution control measures and regional transport. Advances in Atmospheric
604 Sciences 30, 341-353.
605 Watson, J.G., 2002. Visibility: Science and Regulation. Journal of the Air & Waste
606 Management Association 52, 628-713.
607 Watson, J.G., Chow, J.C., Chen, L.W.A., Frank, N.H., 2009. Methods to Assess
608 Carbonaceous Aerosol Sampling Artifacts for IMPROVE and Other Long-Term
609 Networks. Journal of the Air & Waste Management Association 59, 898-911.
610 Watson, J.G., Chow, J.C., Frazier, C.A., 1999. X-ray fluorescence analysis of ambient
611 air samples, in: Landsberger, S., Creatchman, M. (Eds.), Vo-Dinh, T., ed.
612 Advances in environmental industrial and process control technologies: v. 1 ed.
613 Gordon and Breach Science Publishers, Amsterdam, The Netherlands, pp. 67-96.
614 Watson, J.G., Chow, J.C., Lowenthal, D.H., Antony Chen, L.W., Shaw, S., Edgerton,
615 E.S., Blanchard, C.L., 2015. PM2.5 source apportionment with organic markers in
616 the Southeastern Aerosol Research and Characterization (SEARCH) study.
617 Journal of the Air & Waste Management Association 65, 1104-1118.
618 Yao, X., Fang, M., Chan, C.K., 2002. Size distributions and formation of dicarboxylic
619 acids in atmospheric particles. Atmospheric Environment 36, 2099-2107.
620 Yao, X., Lau, A.P.S., Fang, M., Chan, C.K., Hu, M., 2003a. Size distributions and
621 formation of ionic species in atmospheric particulate pollutants in Beijing, China:
622 1—inorganic ions. Atmospheric Environment 37, 2991-3000.
623 Yao, X.H., Fang, M., Chan, C.K., 2003b. The size dependence of chloride depletion in
624 fine and coarse sea-salt particles. Atmospheric Environment 37, 743-751.

625 Yau, P.S., Lee, S.C., Cheng, Y., Huang, Y., Lai, S.C., Xu, X.H., 2013. Contribution of
626 ship emissions to the fine particulate in the community near an international port
627 in Hong Kong. Atmospheric Research 124, 61-72.
628 Yu, H., Wu, C., Wu, D., Yu, J.Z., 2010. Size distributions of elemental carbon and its
629 contribution to light extinction in urban and rural locations in the pearl river delta
630 region, China. Atmospheric Chemistry and Physics 10, 5107-5119.
631 Zhang, R., Jing, J., Tao, J., Hsu, S.C., Wang, G., Cao, J., Lee, C.S.L., Zhu, L., Chen,
632 Z., Zhao, Y., Shen, Z., 2013. Chemical characterization and source apportionment
633 of PM2.5 in Beijing: seasonal perspective. Atmospheric Chemistry and Physics 13,
634 7053-7074.
635 Zhou, S., Wang, T., Wang, Z., Li, W., Xu, Z., Wang, X., Yuan, C., Poon, C.N., Louie,
636 P.K.K., Luk, C.W.Y., Wang, W., 2014. Photochemical evolution of organic
637 aerosols observed in urban plumes from Hong Kong and the Pearl River Delta of
638 China. Atmospheric Environment 88, 219-229.
639 Zhuang, H., Chan, C.K., Fang, M., Wexler, A.S., 1999a. Formation of nitrate and
640 non-sea-salt sulfate on coarse particles. Atmospheric Environment 33, 4223-4233.
641 Zhuang, H., Chan, C.K., Fang, M., Wexler, A.S., 1999b. Size distributions of
642 particulate sulfate, nitrate, and ammonium at a coastal site in Hong Kong.
643 Atmospheric Environment 33, 843-853.
644
645
646

647 Table 1. Meteorological characteristics during each sampling dates

Seasons	Sampling date	Prevail wind [a]	Wind speed (m/s)	Temperature (°C)	Relative humidity %
August/September (summer), 2011	August 4th-5th, 2011	SW	11.40	32	69
	August 22nd -23rd, 2011	SW	11.20	32	71
	August 24th – 25th, 2011	NE	11.20	32	72
	August 29th – 30th, 2011	NW	16.20	34	64
	September 6th -7th, 2011	SE	12.70	32	71
	September 8th – 9th, 2011 (blank)	SE	6.38	30	76
November/December (fall), 2011	November 3rd – 4th, 2011	NE	6.04	28	68
	November 8th – 9th, 2011	NE	10.63	22	80
	November 14th – 15th, 2011	NE	8.85	25	68
	November 21st – 22nd, 2011	NE	10.04	22	60
	November 25th – 26th, 2011	NE	10.6	22	60
	December 1st – 2nd, 2011	N	9.56	16	57
	December 3rd – 4th, 2011 (blank)	N	7.74	18	80
February/March (winter), 2012	February 2nd – 3rd, 2012	NE	8.89	16	70
	February 9th – 10th, 2012	E	8.92	14	79
	February 15th – 16th, 2012	NE	5.08	20	85
	February 20th – 21st, 2012	NE	10.01	18	66
	February 27th – 28th, 2012	NE	7.97	10	80
	March 2nd – 3rd, 2012	NE	5.16	22	83
	March 4th – 5th, 2012 (blank)	NE	6.36	18	89
May (spring), 2012	May 2nd – 3rd, 2012	SW	7.83	30	74
	May 9th – 10th, 2012	SW	6.86	31	69
	May 14th – 15th, 2012	SE	3.11	30	75
	May 21st – 22nd, 2012	SE	11.52	27	67
	May 24th – 25th, 2012	E	8.33	28	75
	May 30th – 31st, 2012	E	6.08	29	75
	June 1st – 2nd, 2012 (blank)	SE	10.36	27	82

648 [a] refer to prevail wind direction, N-North, NE-Northeast, E-East, SE-Southeast, S-South,
649 SW-Southwest, W-West, NW-Northwest.

650

651

652

653

654

655 **Table 2.** Seasonal $PM_{1.8}$ and PM_{10} concentrations in Tung Chung, Hong Kong

Seasons (N=23)	$PM_{1.8}$ $\mu g/m^3$	PM_{10} $\mu g/m^3$	$PM_{1.8}/PM_{10}$
August/September (summer), 2011			
Clean day	19 ± 8	23 ± 7	0.83 ± 0.02
Episode day	62 ± 8	80 ± 13	0.78 ± 0.04
average	38 ± 20	47 ± 27	0.81 ± 0.06
November/December (fall), 2011			
average	37 ± 13	53 ± 17	0.70 ± 0.09
February/March (winter), 2012			
average	34 ± 11	48 ± 11	0.71 ± 0.08
May (spring), 2012			
average	26 ± 7	39 ± 11	0.66 ± 0.03

656

657

658

659 **Table 3.** Fraction of PM source factors in each size mode

Sources	Source makers	Condensation mode (0.1 – 0.56 μm)	Droplet mode (0.56 – 1.8 μm)	Coarse mode (1.8 – 10 μm)
Residual oil combustion	V	21%	N.A.	N.A.
Engine exhaust	EC, OC	26%	14%	N.A.
Coal/Biomass burning	As, Pb, K^+	16%	2%	N.A.
Secondary sulfate	NH_4^+, SO_4^{2-}	37%	24%	N.A.
Secondary nitrate	NO_3^-, K^+	N.A.	13%	N.A.
Incineration	Cu, Zn, OC	N.A.	6%	N.A.
Industry	Mn, Cs	N.A.	19%	19%
Sea salt	Cl, Na, Mg	N.A.	15%	52%
Soil	Si, Al, Fe, Ti, Ca, Fe	N.A.	7%	29%

660

661

Figure Captions

Fig. 1. Location of sampling site, at the Tung Chung monitoring station (TC), Hong Kong

Fig. 2. Time series of PM_{10} concentrations (Particle size modes are defined as: 0.056 -0.1 μm for nucleation mode, 0.1-0.56 μm for condensation mode, 0.56-1.8 μm for droplet mode, and 1.8-10 μm coarse mode)

Fig. 3. Reconstructed PM_{10} mass for: a) summer, b) fall, c) winter and d) spring. The components include, sulfate, nitrate, ammonium, Particulate organic matters ($POM = 1.8 \times OC$), EC, water-soluble potassium, trace element oxides ($TEO = 1.3 \times [0.5 \times (Sr + Ba + Mn + Co + Rb + Ni + V) + 1.0 \times (Cu + Zn + Mo + Cd + Sn + Sb + TI + Pb + As + Se + Ge + Cs + \mathrm{Ga})]$, sea salt ($sea\ salt = 1.47 \times \mathrm{Na^+ + Cl^-}$), soil ($soil = 2.20 \times Al + 2.49 \times Si + 1.63 \times Ca + 2.42 \times Fe + 1.94 \times Ti$)

Fig. 4. Resolved particle mass size distributions for: a) condensation mode, b) droplet mode, and c) coarse mode in PMF

Fig. 5. Average size distributions for: a) sulfate, b) nitrate, c) ammonium, d) water-soluble potassium, e) chloride, f) EC, and g) OC

Fig. 6. Size-fractionated: a) sulfur oxidation ratio (SOR); and b) nitrogen oxidation ratio (NOR) in four seasons

Fig. 7. a) Reconstructed PM mass clean (20.98 μg/m^3) on August 20th, starting episode (71.96 μg/m^3) on August 24th, and ending episode (88.63 μg/m^3) on August 29th; Abundances of each particle size modes in PM_{10} and air trajectory patterns are also shown; and b) Size-fractionated SOR value in clean and episode days

Fig. 8. Source factors for: a) condensation, b) droplet, and c) coarse mode; Chemical species in condensation mode for PMF are NH_4^+, K^+, NO_3^-, SO_4^{2-}, OC, EC, Na, Mg, Al, Cl, Ca, V, Mn, Fe, Cu, Zn, As, Br, Cs, Ba and Pb. The chemical species in droplet mode contains NH_4^+, K^+, NO_3^-, SO_4^{2-}, OC, EC, Na, Mg, Al, Si, Cl, Ca, Ti, Mn, Fe, Cu, Zn, As, Br, Cs, Ba and Pb. In addition, chemical species in coarse mode are NH_4^+, K^+, NO_3^-, SO_4^{2-}, OC, EC, Na, Mg, Al, Si, Cl, Ca, Ti, Mn, Fe, Cu, Zn, Cs, Ba and Pb.

Fig. 9. Source contribution estimates for condensation, droplet, and coarse modes

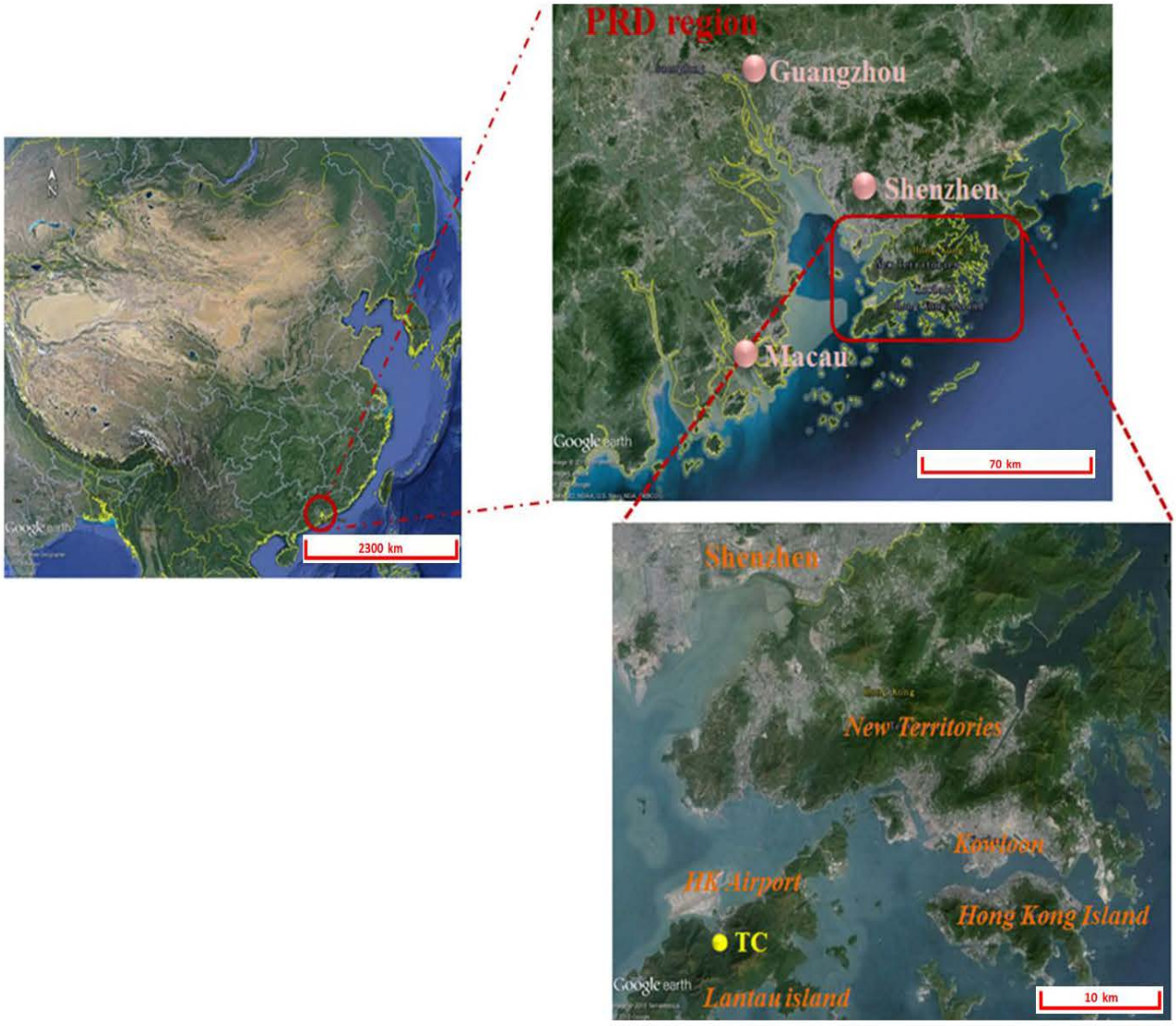

696

697 **Fig. 1**

698

699

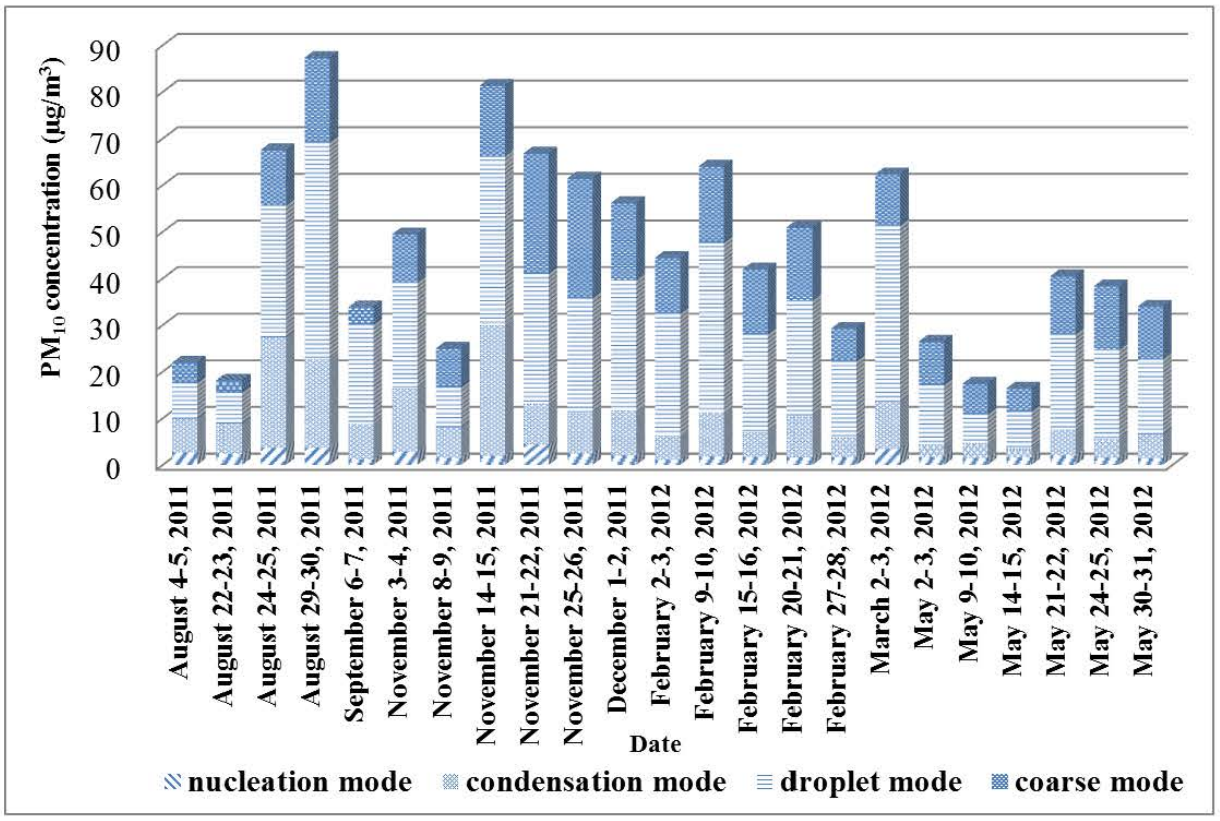

700

701

702

703

704

705 **Fig. 2**

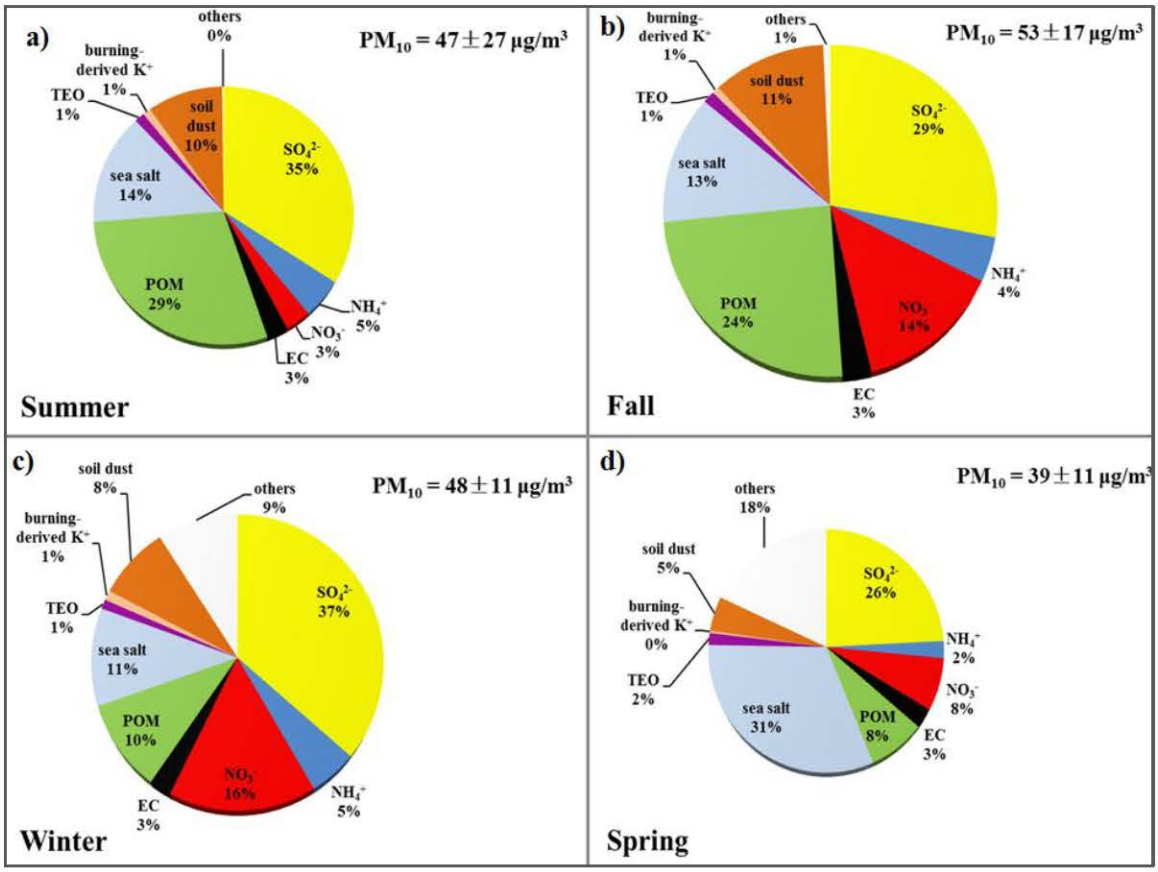
a)
PM10 = 47±27 μg/m3
others 0%
burning-derived K+ 1%
TEO 1%
soil dust 10%
SO4 2- 35%
sea salt 14%
POM 29%
NH4+ 5%
NO3- 3%
EC 3%
Summer
b)
PM10 = 53±17 μg/m3
burning-derived K+ 1%
others 1%
TEO 1%
soil dust 11%
SO4 2- 29%
sea salt 13%
NH4+ 4%
POM 24%
NO3- 14%
EC 3%
Fall
c)
PM10 = 48±11 μg/m3
soil dust 8%
others 9%
burning-derived K+ 1%
SO4 2- 37%
TEO 1%
sea salt 11%
POM 10%
NO3- 16%
EC 3%
NH4+ 5%
Winter
d)
PM10 = 39±11 μg/m3
others 18%
soil dust 5%
SO4 2- 26%
burning-derived K+ 0%
NH4+ 2%
TEO 2%
NO3- 8%
sea salt 31%
POM 8%
EC 3%
Spring

Fig. 3

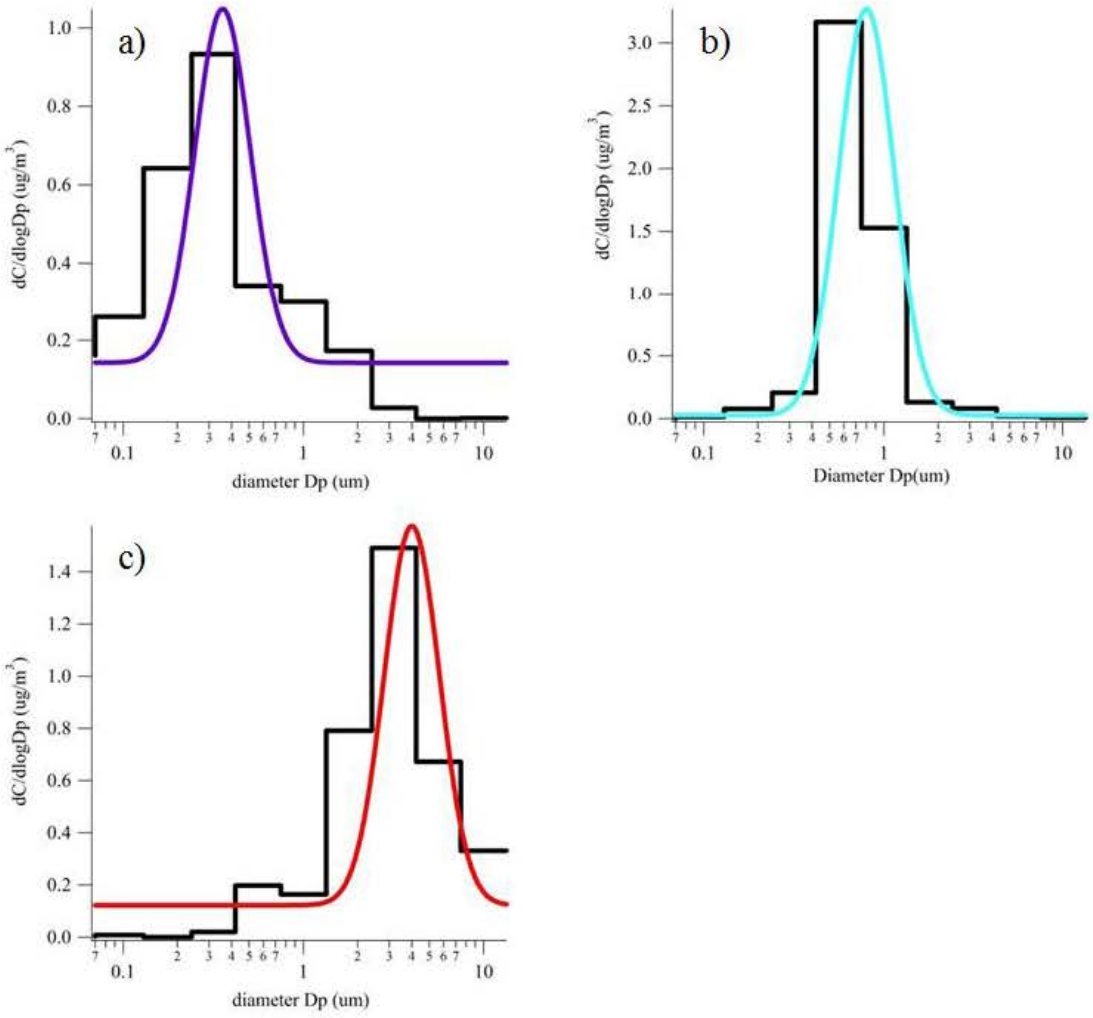

714
715 **Fig. 4**
716

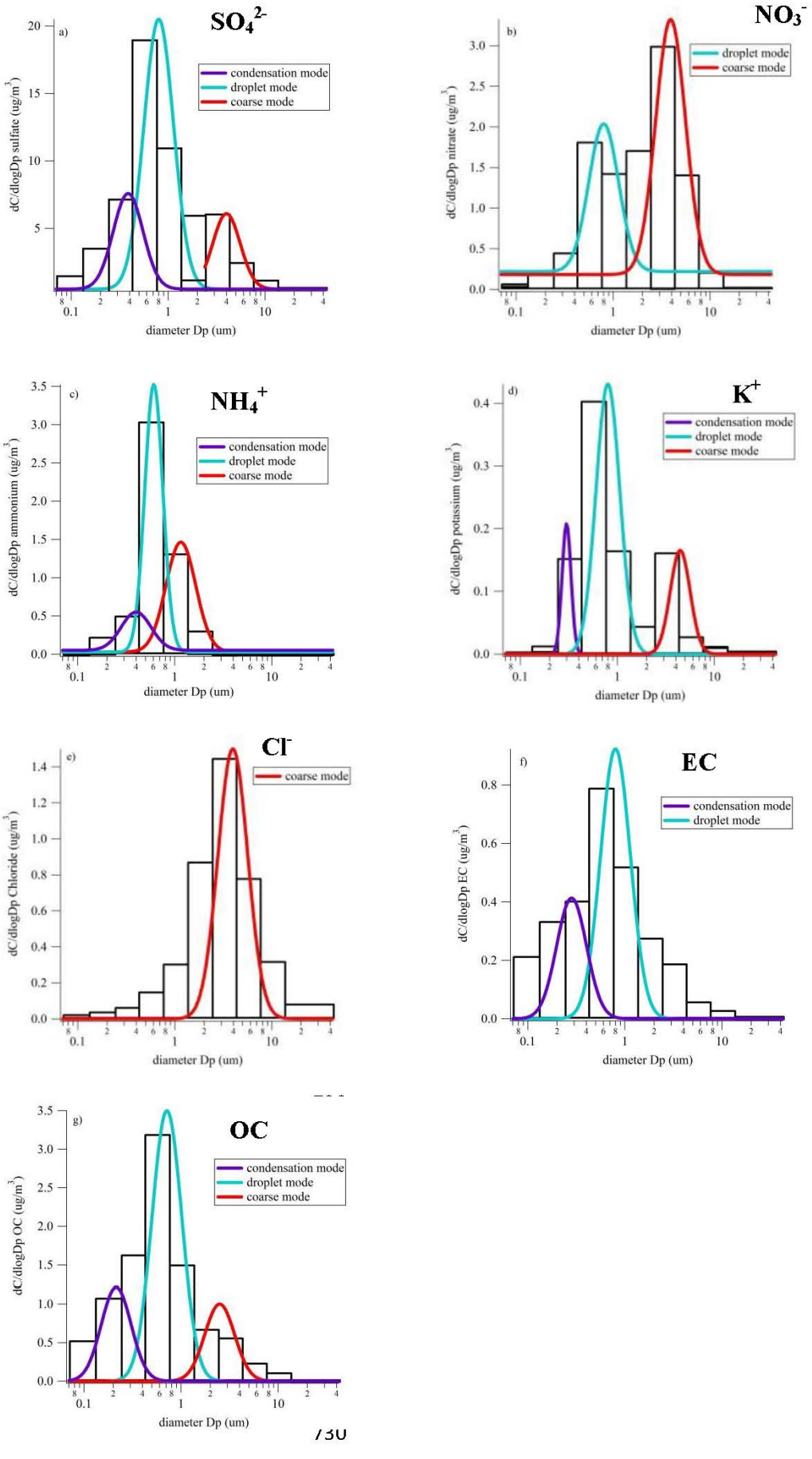
a)
SO_4^{2-}
condensation mode
droplet mode
coarse mode
dC/dlogDp sulfate (ug/m3)
diameter Dp (um)
b)
NO_3^-
droplet mode
coarse mode
dC/dlogDp nitrate (ug/m3)
diameter Dp (um)
c)
NH_4^+
condensation mode
droplet mode
coarse mode
dC/dlogDp ammonium (ug/m3)
diameter Dp (um)
d)
K^+
condensation mode
droplet mode
coarse mode
dC/dlogDp potassium (ug/m3)
diameter Dp (um)
e)
Cl^-
coarse mode
dC/dlogDp Chloride (ug/m3)
diameter Dp (um)
f)
EC
condensation mode
droplet mode
dC/dlogDp EC (ug/m3)
diameter Dp (um)
g)
OC
condensation mode
droplet mode
coarse mode
dC/dlogDp OC (ug/m3)
diameter Dp (um)

Fig. 5

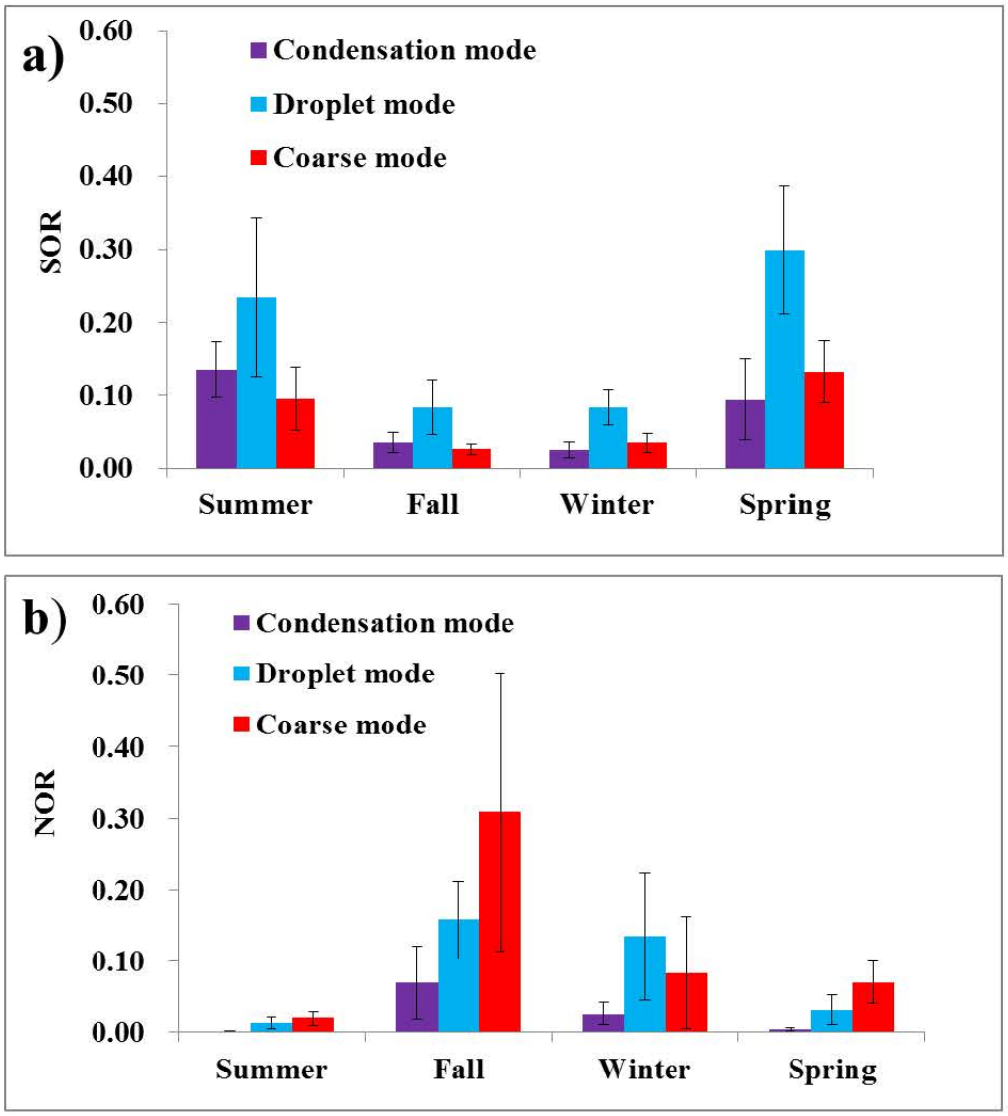
a)
SOR
0.60
0.50
0.40
0.30
0.20
0.10
0.00
Condensation mode
Droplet mode
Coarse mode
Summer
Fall
Winter
Spring
b)
NOR
0.60
0.50
0.40
0.30
0.20
0.10
0.00
Condensation mode
Droplet mode
Coarse mode
Summer
Fall
Winter
Spring

Fig. 6

739 **a)**

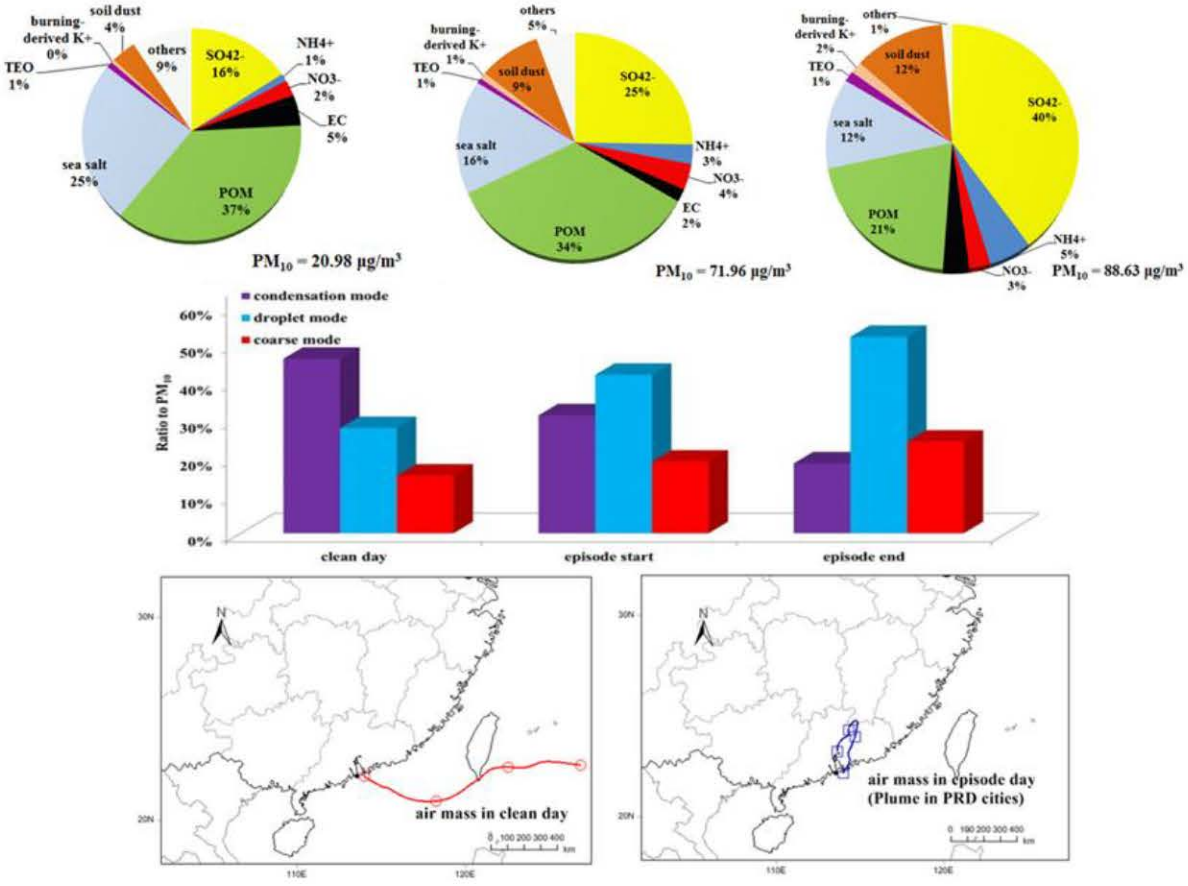

740

741

742 **b)**

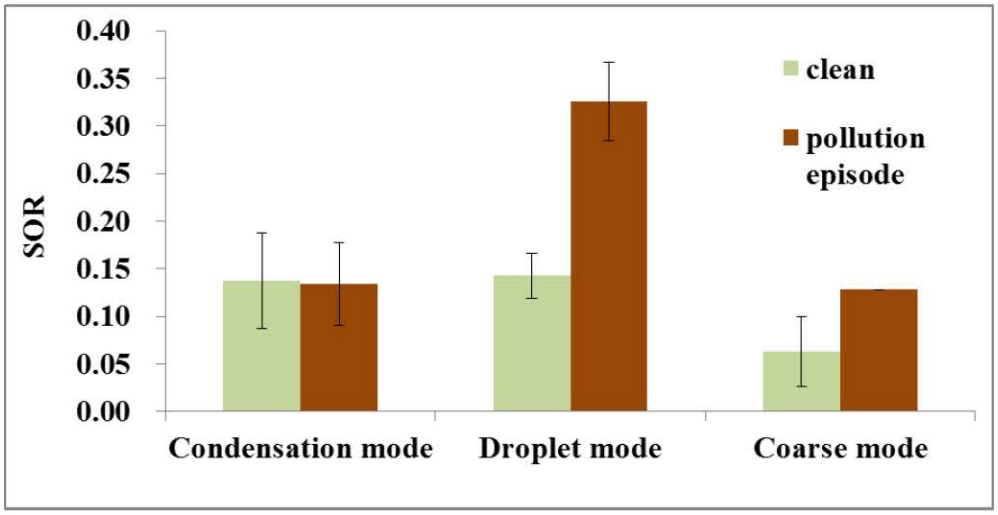

743

744

745 **Fig. 7**

a)

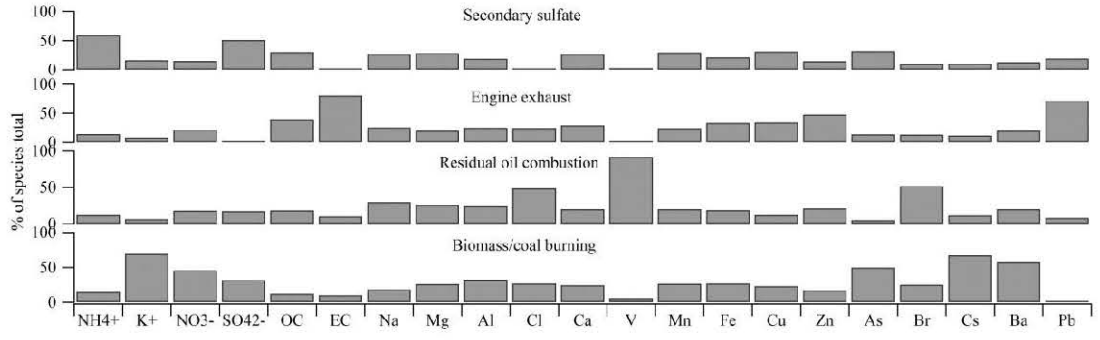
Secondary sulfate
Engine exhaust
Residual oil combustion
Biomass/coal burning
% of species total
100
50
0
NH4+ K+ NO3- SO42- OC EC Na Mg Al Cl Ca V Mn Fe Cu Zn As Br Cs Ba Pb

b)

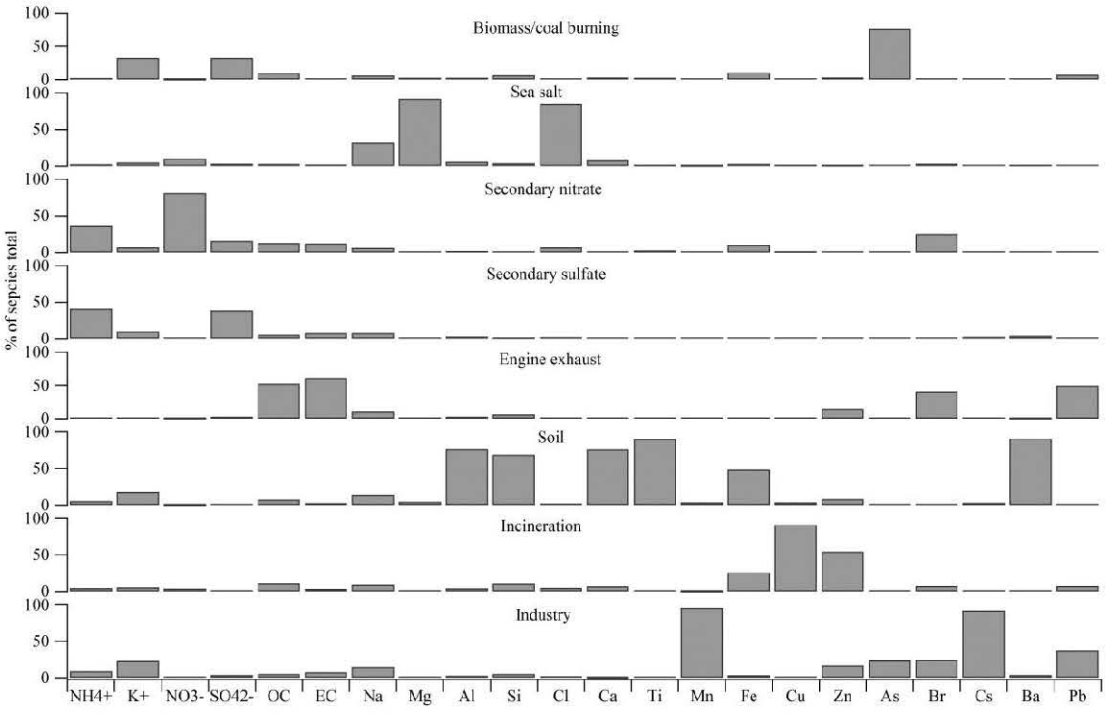
Biomass/coal burning
Sea salt
Secondary nitrate
Secondary sulfate
Engine exhaust
Soil
Incineration
Industry
% of sepcies total
100
50
0
NH4+ K+ NO3- SO42- OC EC Na Mg Al Si Cl Ca Ti Mn Fe Cu Zn As Br Cs Ba Pb

c)

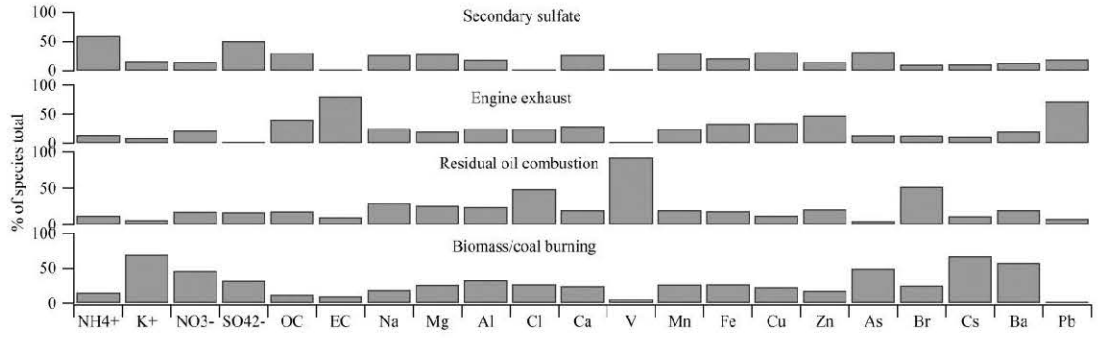
Secondary sulfate
Engine exhaust
Residual oil combustion
Biomass/coal burning
% of species total
100
50
0
NH4+ K+ NO3- SO42- OC EC Na Mg Al Cl Ca V Mn Fe Cu Zn As Br Cs Ba Pb

Fig. 8

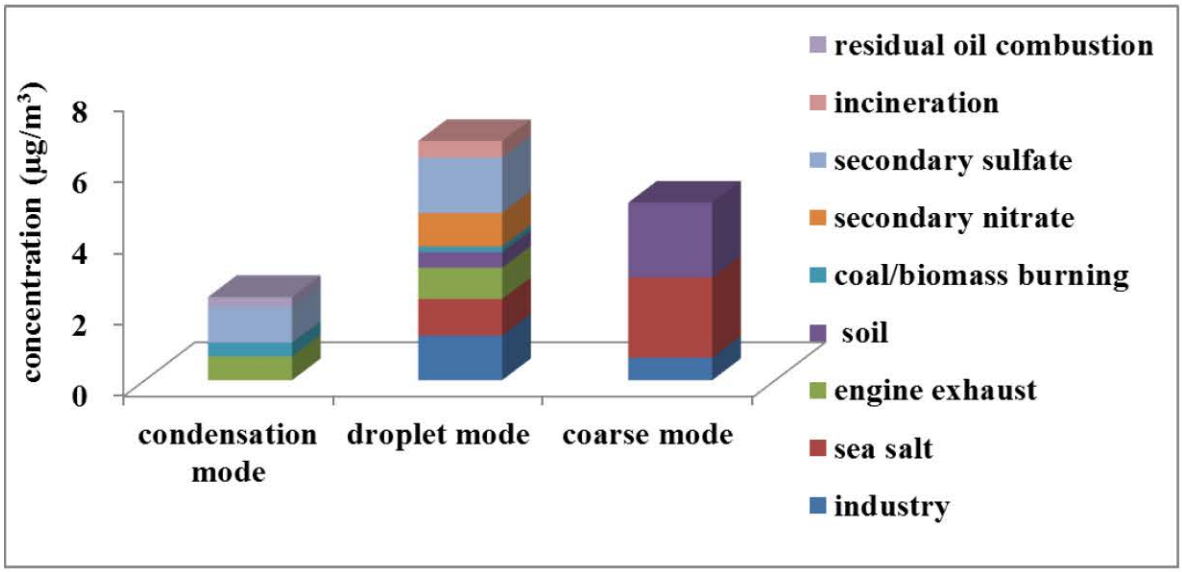

755
756
757 **Fig. 9**
758